Catalytic Implications from the *Drosophila* Protein L-Isoaspartyl Methyltransferase Structure and Site-Directed Mutagenesis[†,‡]

Eric J. Bennett,[§,||] Jens Bjerregaard,[§,||] James E. Knapp,[§,⊥] David A. Chavous,[||] Alan M. Friedman,[#] William E. Royer, Jr.,[⊥] and Clare M. O'Connor*[,||]

Biology Department, Boston College, Chestnut Hill, Massachusetts 02467, Department of Biochemistry and Molecular Pharmacology, University of Massachusetts Medical School, Worcester, Massachusetts 01655, and Department of Biological Sciences, Purdue University, West Lafayette, Indiana 47907

Received May 26, 2003; Revised Manuscript Received September 7, 2003

ABSTRACT: Protein L-isoaspartyl methyltransferases (PIMT; EC 2.1.1.77) catalyze the *S*-adenosylmethionine-dependent methylation of L-isoaspartyl residues that arise spontaneously in proteins with age, thereby initiating a repair process that restores the normal backbone configuration to the damaged polypeptide. In *Drosophila melanogaster*, overexpression of PIMT in transgenic flies extends the normal life span, suggesting that protein damage can be a limiting factor in longevity. To understand structural features of the *Drosophila* PIMT (dPIMT) important for catalysis, the crystal structure of dPIMT was determined at a resolution of 2.2 Å, and site-directed mutagenesis was used to identify the role of Ser-60 in catalysis. The core structure of dPIMT is similar to the modified nucleotide-binding fold observed in PIMTs from extreme thermophiles and humans. A striking difference of the dPIMT structure is the rotation of the C-terminal residues by 90° relative to the homologous structures. Effectively, this displacement generates a more open conformation that allows greater solvent access to *S*-adenosylhomocysteine, which is almost completely buried in other PIMT structures. The enzyme may alternate between the open conformation found for dPIMT and the more closed conformations described for other PIMTs during its catalytic cycle, thereby allowing the exchange of substrates and products. Catalysis by dPIMT requires the side chain of the conserved, active site residue Ser-60, since substitution of this residue with Thr, Gln, or Ala reduces or abolishes the methylation of both protein and isoaspartyl peptide substrates.

Protein carboxyl *O*-methyltransferase activities (PIMT)[1] with a specificity for L-isoaspartyl residues (EC 2.1.1.77) have been identified in organisms from all domains of life (*1*, *2*). These strongly conserved enzymes catalyze the transfer of methyl groups from *S*-adenosylmethionine (AdoMet) to isoaspartyl residues in a large number of peptides and proteins, resulting in the production of an isoaspartyl methyl ester and *S*-adenosylhomocysteine (AdoHcy). The isoaspartyl residues that are modified in PIMT-catalyzed reactions arise posttranslationally in cellular proteins from the spontaneous deamidation of protein asparaginyl residues and isomerization of protein aspartyl residues (*3*−*5*). The appearance of isoaspartyl residues in proteins, involving the addition of a carbon to the polypeptide backbone, can severely diminish the enzymatic activity of the affected protein (*6*, *7*). Evidence to date suggests that PIMT functions in the repair of its isoaspartyl-containing substrates, possibly preventing the accumulation of dysfunctional proteins in cells. Biochemical experiments have shown that methylation of isoaspartyl peptides by PIMT in vitro is followed by the spontaneous reversion of a significant fraction of the methylated isoaspartyl residues to normal aspartyl residues (*8*, *9*). In the case of several protein substrates, restoration of the normal polypeptide backbone is accompanied by the partial restoration of enzymatic activity (*6*, *10*).

Because of the heterogeneity of methyl-accepting substrates for PIMT in intact cells (*11*) and the low fractional representation of isoaspartyl forms of cellular proteins (*12*, *13*), it has not been possible to demonstrate the conversion of an isoaspartyl-containing protein to its normal counterpart in vivo. Other evidence, however, strongly supports a role for PIMT in cellular protein repair. In microinjection experiments with *Xenopus laevis* oocytes, isoaspartyl-containing forms of calmodulin were much more rapidly proteolyzed following microinjection than normal calmodulin. The stability of the isoaspartyl-containing calmodulin could be significantly increased, however, by premethylation with purified PIMT prior to injection, consistent with a role for PIMT in protein repair (*14*). Transgenic knockout animals have provided additional circumstantial evidence for PIMT-

[†] This work was supported by National Institutes of Health Grants AG08109 to C.M.O., AG14838 to A.M.F., and DK43323 to W.E.R., National Science Foundation Grant MCB-0233538 to C.M.O., a Boston College Research Expense Grant to C.M.O., and a Pfizer Summer Undergraduate Research Fellowship to E.J.B.

[‡] The coordinates of dPIMT have been deposited in the Protein Data Bank under the accession number 1R18.

* To whom correspondence should be addressed. Phone: 617-552-2553. Fax: 617-552-2011. E-mail: oconnocn@bc.edu.

[§] These three authors contributed equally to this work and are listed alphabetically.

[||] Boston College.

[⊥] University of Massachusetts Medical School.

[#] Purdue University.

[1] Abbreviations: PIMT, protein carboxyl methyltransferase; dPIMT, *Drosophila* PIMT; AdoMet, *S*-adenosylmethionine; AdoHcy, *S*-adenosylhomocysteine; MTase, methyltransferase; PMSF, phenylmethanesulfonyl fluoride; DTT, dithiothreitol; GST, glutathione *S*-transferase; rms, root mean square.

10.1021/bi034891+ CCC: $25.00
Published on Web 10/16/2003

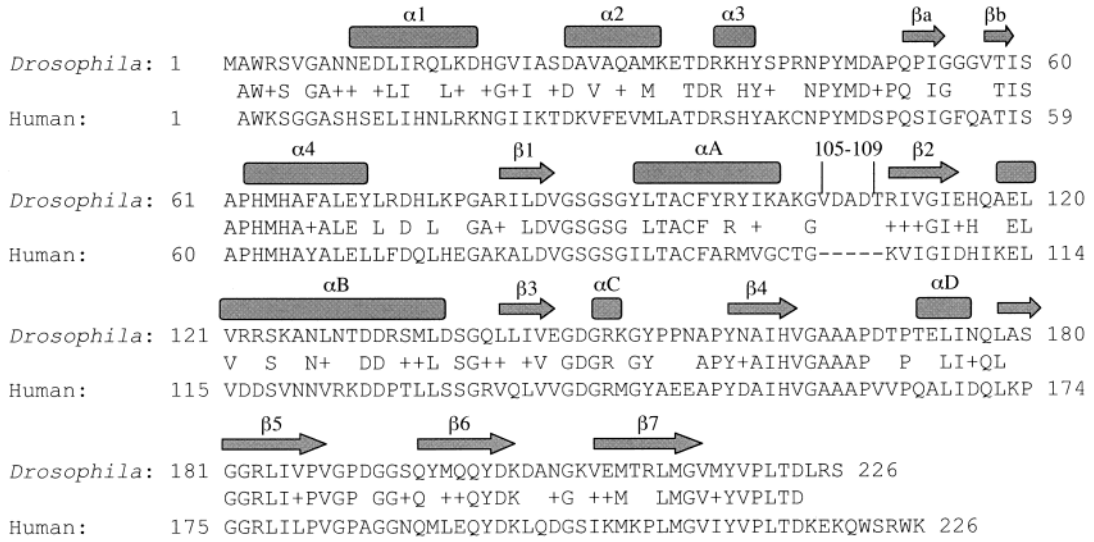

FIGURE 1: Structure-based alignment of *Drosophila* and human PIMT sequences. The primary sequences of dPIMT and human PIMT were aligned using BLAST. Secondary structure elements in *Drosophila* PIMT were assigned using PROCHECK (*40*). Secondary structure elements were named using the scheme described by Skinner et al. (*22*).

mediated protein repair. In several studies, isoaspartyl-containing proteins show significant accumulations over time in the tissues of transgenic mice deficient in PIMT activity compared to control animals (*15*, *16*). The accumulation of damaged proteins may, in fact, be a causative factor in the fatal epileptic seizures experienced by these mice at 20−60 days of age. Similar, but smaller, accumulations of isoaspartyl proteins were noted in *Caenorhabditis elegans* deficient in PIMT, which also displayed a slightly reduced ability to survive in the dauer phase (*17*).

We have been interested in using *Drosophila melanogaster* as a genetic model to study PIMT function and potential modifiers of PIMT activity. Taking advantage of the GAL4-UAS system (*18*) to genetically manipulate PIMT levels in vivo, we have shown that overexpression of PIMT causes a significant extension of the normal life span (*19*). The longevity effect was restricted, however, to flies raised at slightly elevated temperatures of 29 °C and above, conditions which would be expected to increase the rate of isoaspartyl generation in cellular proteins. The results suggested that life span may be limited by the accumulation of unrepaired cellular proteins and raised the possibility that *Drosophila* could be a useful model in which to identify structural features of PIMT important for its effects on longevity.

As the first step toward this goal, we have determined the crystal structure of *Drosophila* PIMT (dPIMT). Overall, the sequence of dPIMT is 56% identical to that of human PIMT (*20*, *21*), which was used as the search model for molecular replacement, but identities are much higher in strongly conserved regions (Figure 1). The dPIMT structure includes the core fold and substrate binding cleft previously identified in the crystal structures of PIMTs from *Thermatoga maritima* (*22*), *Pyrococcus furiosus* (*23*), and human (*20*, *21*). A novel feature of dPIMT is a more open conformation at the C-terminus, which has implications for substrate binding. Mutagenesis of Ser-60, a conserved residue on one rim of the substrate binding cleft, reduces or eliminates enzymatic activity, indicating the importance of this residue to the enzymatic mechanism.

EXPERIMENTAL PROCEDURES

Enzyme Overexpression and Purification. An overexpression vector for the GST-dPIMT fusion protein was constructed by ligating an *Eco*RI fragment containing the complete coding sequence of *Drosophila PIMT* (*24*) into the *Eco*RI site of pGEX2-T (Amersham Biosciences, Piscataway, NJ). DNA sequencing confirmed that the *dPIMT* coding sequence had been cloned in frame to the *Schistosoma japonicum* GST coding sequence and that the two domains were separated by a linker sequence containing a thrombin cleavage site. GST-dPIMT overexpression was induced by incubating a 1 L culture of transformed BL21(DE3) *Escherichia coli* overnight at 16 °C in 2× YTA medium containing 0.1 mM isopropyl β-D-thiogalactoside. Cells were concentrated by centrifugation at 8000*g* for 5 min and resuspended in 37 mL of 10 mM Tris-HCl, pH 8.0, 1 mM EDTA, 5 mM NaCl, 0.1 mM dithiothreitol (DTT), 0.1 mM phenylmethanesulfonyl chloride (PMSF), and 0.2 mg/mL lysozyme. Cells were lysed by three cycles of freezing and thawing, followed by three 10 s bursts of sonication using a Virsonic 60 sonicator with a 2.5 mm probe at a setting of 6 W. Samples were clarified by centrifugation at 10550*g* for 15 min, and the GST-dPIMT fusion protein was purified using the GST purification module (Amersham Biosciences, Piscataway, NJ). Briefly, the lysate was diluted with 240 mL of phosphate-buffered saline (PBS: 150 mM NaCl, 10 mM sodium phosphate, pH 7.4) containing 0.1 mM PMSF, 0.1 mM DTT, and 1% Triton X-100. The diluted lysate was incubated with approximately 5 mL of glutathione affinity resin for 4 h at room temperature with constant shaking. The resin was then collected into a 0.5 × 5.5 cm column and washed with 50 mL of PBS. To purify dPIMT free of GST, 1 mL of PBS containing 20 units of thrombin was applied to the column, and the column was allowed to stand overnight at room temperature. PIMT activity was eluted from the column in PBS, and the column was treated with an additional 20 units of thrombin for 2 h. Once again, PIMT activity was eluted with PBS and combined with the PIMT activity liberated during the first round of thrombin cleavage. To remove residual thrombin and occasional contaminants,

samples were first dialyzed against 1 L of 20 mM Tris-HCl, pH 8, 0.2 mM EDTA, and 100 μM PMSF at 4 °C and then applied to a column (0.5 × 5.5 cm) of Q-Sepharose Fast Flow equilibrated in the same buffer (*25*). The column was washed with 15 mL of starting buffer and eluted with 40 mL of a 0−200 mM NaCl gradient in the same buffer at a flow rate of 1 mL/min. Peak fractions containing PIMT activity were pooled and concentrated using Centricon-10 concentrators (Millipore Corp., Bedford, MA). Protein concentrations were determined using Coomassie Blue dye binding assays (Bio-Rad Corp., Hercules, CA). The purity of the samples was monitored by SDS−PAGE. The procedure typically yielded 4−9 mg of protein/L of bacterial culture with 99% purity.

Because the calculated mass of dPIMT is virtually identical to the mass of 25.5 kDa predicted for *S. japonicum* GST, several control experiments were done to establish that the dPIMT was not contaminated with GST (data not shown). First, GST activity was measured in the fractions using a colorimetric assay and compared to a standard curve established for purified GST. GST activity was undetectable in these assays, establishing an upper limit for GST contamination of 0.01%. In addition, no GST could be detected in samples of dPIMT following two-dimensional electrophoresis or by Western blotting using an anti-GST antibody. Finally, tryptic peptide analysis of purified dPIMT by MALDI-TOF mass spectroscopy revealed only peptides expected for dPIMT and none of the peptides expected for GST.

Crystallization and Data Collection. Crystallization screens were conducted by vapor diffusion using the sitting drop method. A reservoir containing 500 μL of mother liquor was allowed to equilibrate with a 10 μL sitting drop, constructed by combining equal volumes of mother liquor and concentrated protein. Crystal Screen kits 1 and 2 (Hampton Research, Laguna Niguel, CA) and Wizard Screens 1 and 2 (Emerald BioStructures, W. Bainbridge Island, WA) were used to identify potential crystallization conditions. Diffraction-quality crystals grew in drops containing 6 mg/mL PIMT with a 2:1 mol/mol ratio of AdoHcy:PIMT above a reservoir containing 35% ethanol and 100 mM Tris-HCl, pH 7.5 at 4 °C. Under these conditions, large crystals (0.5 × 0.25 × 0.15 mm) appeared within 4 days. PIMT crystals show the symmetry of spacegroup *C*2 with cell dimensions of a = 72.07 Å, b = 45.25 Å, c = 61.24 Å, and β = 102.90°. The cell dimensions are consistent with a single monomer in the asymmetric unit based on the Matthews coefficient (V_M) of 1.95 Å^3/Da (*26*), which gives a calculated solvent content of 37%.

X-ray diffraction data were measured at room temperature with an R-AXIS IV image plate detector mounted on a Rigaku generator equipped with osmic mirror optics (Molecular Structure Corp., The Woodlands, TX). The data set was collected from one crystal using a crystal to film distance of 70 mm, an oscillation angle of 1.5°, and an exposure time of 10 min per frame. X-ray data were processed and merged using the HKL package (*27*) and converted to structure factors with Truncate (*28*). The data from 65 images resulted in a data set that is 89% complete to 2.2 Å resolution, with an overall R_{sym} of 8.8% and an overall $I/\sigma(I)$ of 11.4. The outer resolution shell includes 44.6% of the theoretically expected reflections with an $I/\sigma(I)$ greater than 2. At this point, 5% of the reflections were set aside for the calculation of a free *R*-factor.

Structure Solution and Refinement. The phase problem was solved by the molecular replacement method using the PIMT from human (*20*) as the search model (Protein Data Bank accession number 1I1N). This model was placed in the fly PIMT unit cell with the AMORE package (*29*). Multiple rounds of computational refinements were then carried out with the program CNS (*30*) using rigid-body refinement, simulated annealing (*31*), and grouped *B*-factor refinement, in which main chain and side chain *B*-factors are optimized for each residue. Between each round of refinement, the model was fitted to $2F_o - F_c$, sigmaA-weighted electron density maps (*32*) with the program O (*33*). Water molecules were added with the picking algorithms of CNS during the eighth round of refinement. The last round of refinement included real-space refinement (*34*) followed by CNS refinement.

The initial model was truncated to alanines during the first round of refinement. Side chains were then added back into the model and into simulated annealing, $2F_o - F_c$ omit maps during the first round of model fitting with the program O (*33*). The first and last 6 residues of the protein and the residues that form the loop connecting αA and β2 (residues 105−109) were omitted from the model after the first round of refinement because of the poor electron density in these regions of the map. The 105−109 loop was added after the second round of model building, and the N- and C-terminal ends were added after the fourth round of refinement. All three segments were rebuilt into simulated annealing omit density. AdoHcy was left out of the initial calculations but was added after the seventh round of refinement. The refined model includes residues 1−221 but lacks the last five residues of the dPIMT sequence, which were not present in the electron density. This model does not include residue 191, and the side chains of Arg-43 and Ser-194 have been truncated to alanine. The model also includes two N-terminal residues remaining after thrombin digestion of the GST linker sequence, with both residues being truncated to alanine. The four remaining linker residues were not present in the electron density. The refined model also includes the cofactor AdoHcy and 73 water molecules.

All superposition calculations were made with the program LSQMAN (*35*). This program was also used to make models of dPIMT−peptide substrate complexes by superimposing the coordinates of the *Pyrococcus* PIMT−peptide complex upon the coordinates of dPIMT. This process brought the peptide substrate into the dPIMT active site without any additional manual adjustments. Models of two mutant dPIMTs were constructed with the computer software O (*33*). The S60T and S60Q mutations were initially introduced into dPIMT on the basis of the preferred rotamers. The χ1 (S60T) or both the χ1 and χ2 angles (S60Q) were manually adjusted to minimize poor steric contacts. The peptide substrate was simulated for each structure on the basis of the superposition calculations described above. Solvent-accessible surface area calculations were made with the program Surface from the CCP4 package (*36*).

Methyltransferase Assays. *S*-Adenosyl-L-[*methyl*-^{3}H]methionine ([^{3}H]AdoMet; 15 Ci/mmol) was obtained from New England Nuclear (Billerica, MA) and adjusted to a specific activity of 1 Ci/mmol with nonradioactive AdoMet (Sigma

Chemical Co., St. Louis, MO). Reaction mixtures (25 μL) containing 40 nM PIMT, 6 μM [^{3}H]AdoMet (1.0 Ci/mmol), and isoaspartyl substrates in 25 mM MES, pH 6.5, were incubated at 37 °C for various lengths of time, as indicated in the figure legends. Substrates included ovalbumin and the isoaspartyl peptides KASA(iso-D)LAKY and VYP(iso-D)-HA, which were diluted with 25 mM MES, pH 6.5, to give final substrate concentrations of 0.5−450 μM for peptides or 5−450 μM for ovalbumin. Synthetic peptide substrates were the generous gifts of Dr. Steven Clarke (Department of Chemistry and Biochemistry, UCLA). Protein and peptide [^{3}H]methyl esters were quantified as described previously (*37*). Kinetic parameters were determined by nonlinear regression of the data points to the Michaelis−Menten equation using KaleidaGraph (Synergy Software, Reading, PA).

Site-Directed Mutagenesis. The unique site elimination method (*38*) was used to introduce mutations into GST-PIMT according to the instructions accompanying the Transformer mutagenesis kit (Clontech, Palo Alto, CA). One of the two mutagenic primers (Integrated DNA Technologies, Coralville, IA) used in this method, GATGCCTGCAACAATG-GCAAC, eliminated a unique *Pst*I restriction site from the cloning vector. The other mutagenic primers were designed to simultaneously introduce desired mutations into the PIMT-coding sequence and add an *Alu*I cleavage site adjacent to the site of the mutation. The boldface nucleotides in the wild-type sequence GGTGTCACCATC**AGT**GCTCCTCACATG were modified in mutagenic primers to GCA, ACA, and CAA, thus converting the wild-type Ser to Ala, Thr, and Gln, respectively.

RESULTS

Cloning and Overexpression of dPIMT. The GST-PIMT fusion protein was overexpressed and purified by glutathione affinity, as described in Experimental Procedures. Thrombin cleavage of the fusion protein generated dPIMT with a six amino acid extension, GSPGIH, at the N-terminus. The amino acid sequence of dPIMT is shown in Figure 1 together with the sequence of human PIMT for comparison. Regions of highest similarity occur throughout the sequence in areas of structural or functional importance, near the active site or in the core of the protein. A novel feature of dPIMT is the presence of the five amino acid sequence V_{105}DADT$_{109}$, which has no counterpart in any known PIMT.

Structure Determination. The crystal structure of dPIMT was determined by molecular replacement using the human enzyme as the search model and refined at 2.2 Å resolution (Table 1). The refined model has good geometry and is consistent with the observed data, as indicated by a *R*-factor of 0.194 and a free *R*-factor of 0.233 for all reflections between 40 and 2.2 Å resolution. Overall, dPIMT forms a three-layer structure surrounding a central β sheet. Figure 1 shows the secondary structure assignments derived from the dPIMT structure aligned with the human PIMT sequence. The central sheet is composed of seven strands with the topological arrangement 3↑2↑1↑4↑5↑6↓7↑ connected by α helices. Following conventions established for other AdoMet-dependent methyltransferases (MTases), helices within the core MTase domain are assigned letters A through E. Like other PIMTs, dPIMT lacks helix αE (*39*). The helices within the MTase core are positioned such that the central sheet is flanked to the right by helices αC and αD and to the left by helices αA and αB. Four additional helices, α1, α2, α3, and α5, as well as a small, two-stranded, antiparallel β sheet form an N-terminal subdomain that folds next to helices αA and αB (Figure 2, top panel).

Table 1: Data Collection and Refinement Statistics[a]

parameters	values
resolution range (Å)	40.0−2.2
high-resolution bin (Å)	2.28−2.20
reflections	8636 (761)[a]
observations	14628
completeness (%)	89.0 (79.6)
R_{sym}	0.088 (0.232)
$I/\sigma(I)$	11.4 (2.9)
R-factor	0.194 (0.229)
R-free	0.233 (0.257)
no. of non-hydrogen atoms	
protein atoms	1675
AdoHcy atoms	26
solvent atoms	75
average *B*-factors	
main chain atoms (Å^2)	18.6
side chain atoms (Å^2)	25.3
AdoHcy atoms (Å^2)	14.3
solvent atoms (Å^2)	28.9
rms deviation from ideal values	
bonds lengths (Å)	0.005
bond angles (deg)	1.32
Ramachandran plot	
most favored regions (%)	89.1
allowed regions (%)	10.9

[a] Values in parentheses are those for the high-resolution bin.

The αβα MTase fold has been observed in the prokaryotic PIMT homologues from *T. maritima* (*22*) and *P. furiosus* (*23*) as well as in the human homologue (*20,21*). All four PIMT structures share a central sheet with the unique topology 3↑2↑1↑4↑5↑6↓7↑, first identified in the *T. maritima* enzyme. By contrast, the central sheets in AdoMet-dependent MTases with different substrate specificities have a more typical 3↑2↑1↑4↑5↑7↓6↑ topological arrangement for strands 6 and 7 (*39*). Comparison of available PIMT structures indicates that dPIMT is most similar to human PIMT, as indicated by an rms difference of 0.8 Å when the core of human PIMT (170 Cα atoms) is superimposed upon its counterpart from dPIMT (Figure 2, middle panel). The dPIMT structure shows large deviations from all other PIMT structures in the disposition of the N- and C-terminal ends of the protein and in the presence of an extended loop, V_{105}-DADT$_{109}$, between helix αA and strand β2 (Figure 2). This loop, which is marked by the arrow in the top panel of Figure 2, is found only in dPIMT.

The C-terminal end of dPIMT (residues 208−216) occupies a β strand structure followed by a loop with an irregular secondary structure (residues 217−221), which corresponds to one rim of the substrate binding cleft in other PIMT structures. In dPIMT, the C-terminus is oriented about 90° differently from its counterpart in human PIMT. This opens up a cavity between the C-terminal segment and strand βb, which is occupied in the dPIMT crystal lattice by the N-terminal end of a crystallographic 2-fold-related dPIMT (Figure 3). Although the N-terminal segment of dPIMT (residues 1−5) also has an irregular structure, it nonetheless forms six hydrogen bonds between main chain atoms of the crystallographically related C-terminal segment in a manner

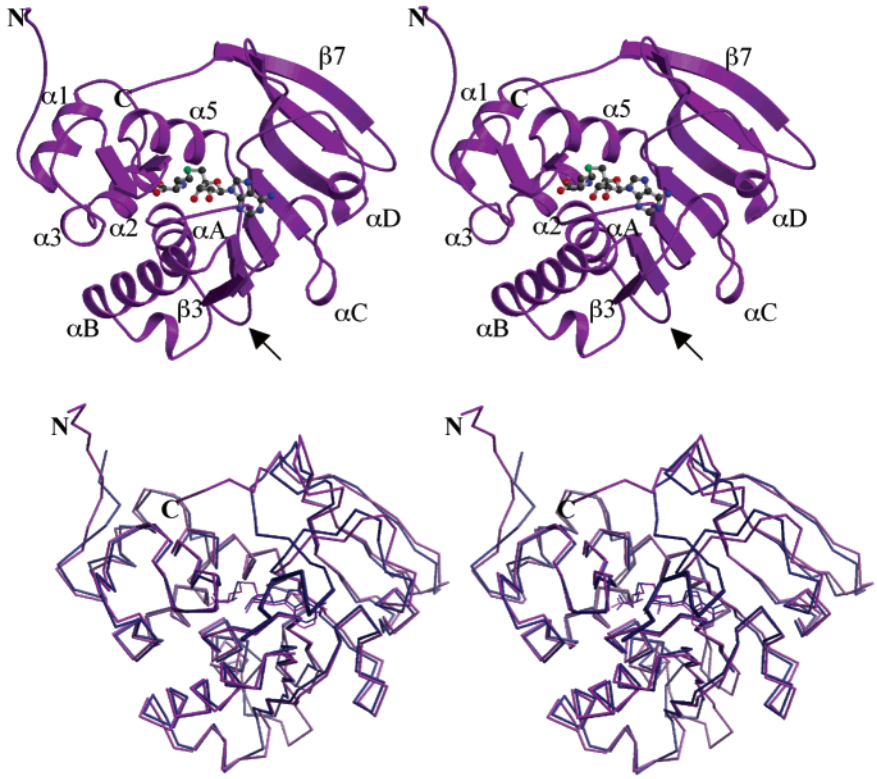

FIGURE 2: *Drosophila* PIMT is structurally similar to PIMTs from other sources. The core structure of dPIMT (top panel) is arranged around a central β sheet and is flanked by a small, two-stranded sheet and a number of helical segments. The superposition (bottom panel) of the core residues from dPIMT (purple) onto the human PIMT structure (blue) gives an rms difference of 0.8 Å for 170 Cα atoms. Addditional superposition of the core residues from dPIMT onto their counterparts *P. furiosus* and *T. maritima* gives respective rms differences of 1.3 and 1.9 Å for 170 Cα atoms (not shown). There are several important differences, located at the N- and C-terminal ends of dPIMT and in the unique $V_{105}DADT_{109}$ loop (arrow) formed between helix αA and strand β2 of dPIMT. The C-terminal end of dPIMT opens up a channel to the solvent that is blocked in the other three PIMT structures. This point leads us to describe this structure as an open conformational form of PIMT. For continuity, all dPIMT residues (including the two residues of the GST tag and the omitted residue at position 191) are included in both parts of Figure 1. This figure and Figures 3, 4, and 6 were made with Bobscript (*43*) and Raster3D (*44*).

that is similar, but not identical, to a β strand. The interaction is further stabilized by a stacking interaction between Tyr-218 from one subunit and Trp-3 from the crystallographically related molecule. An additional hydrogen bond between the Nϵ1 atom of Trp-3 and the main chain carbonyl of Gly-164 positions Trp-3 near the active site such that the Nϵ2 atom of its side chain is 5.7 Å away from the SD atom of the AdoHcy end product and 4.9 Å away from the hydroxyl oxygen of Ser-60. The net result is to position the N-terminal arm so that it occupies a position similar to that of an isoaspartyl peptide substrate in a *P. furiosus* PIMT cocrystal (Figure 3; see Discussion).

Despite the relatively large changes near the active site caused by the orientation of the C-terminus, the AdoHcy product adopts similar conformations in the fly (Figure 4) and human PIMT structures. The most notable difference in AdoHcy binding in the dPIMT structure is a slight reorientation of the homocysteinyl group caused by a small distortion in the bond angle involving the sulfur atom. A large number of interactions are identical in the two structures. These include neutralization of the negative charge of the homocysteinyl carboxyl group by interactions with equivalent His residues and a bridging interaction between the homocysteinyl amino group and equivalent Asp residues mediated by a pair of bound water molecules. Furthermore, the adenine rings of AdoHcy stack on top of equivalent imidazole rings in both structures, and the hydroxyl groups of the nucleotide ribose are hydrogen-bonded with the equivalent Glu residues.

There are two important differences, however, in AdoHcy binding between dPIMT and human PIMT. First, while the O2 atom of the AdoHcy ribose ring in dPIMT is hydrogen-bonded to the side chain of Gln-117, the equivalent Ile-112 in human PIMT is oriented away from the end product. Instead, human PIMT utilizes a hydrogen bond formed between the AdoHcy ribose and the side chain of Gln-221. An equivalent residue to Gln-221 is not present in the fly PIMT sequence. The second difference in AdoHcy binding occurs because the altered position of the C-terminal tail removes a number of binding contacts with one face of the adenine ring in AdoHcy. This exposes this part of the AdoHcy to solvent and opens up a pathway to the exterior of dPIMT. By contrast, solvent access to AdoHcy is much more restricted in other PIMT structures.

Mutagenesis of Ser-60 Reduces Catalytic Activity. The highly conserved sequence $V_{56}ITASAP_{62}$ in dPIMT contains an invariant Ser that is homologous to Ser-75 of *P. furiosus* PIMT, which donates a hydrogen bond to an isoaspartyl side chain in a cocrystal structure (*23*). To determine the catalytic importance of this residue, Ser-60 was replaced with Ala, Thr, or Gln by site-directed mutagenesis. Mutant enzymes were overexpressed and purified using the procedures developed for the wild-type enzyme. The kinetic parameters for the wild-type and mutant enzymes were determined from reactions using a saturating concentration of AdoMet and either ovalbumin or the isoaspartyl peptide KASA(isoD)-LAKY (Figure 5) as the methyl-accepting substrate. Data

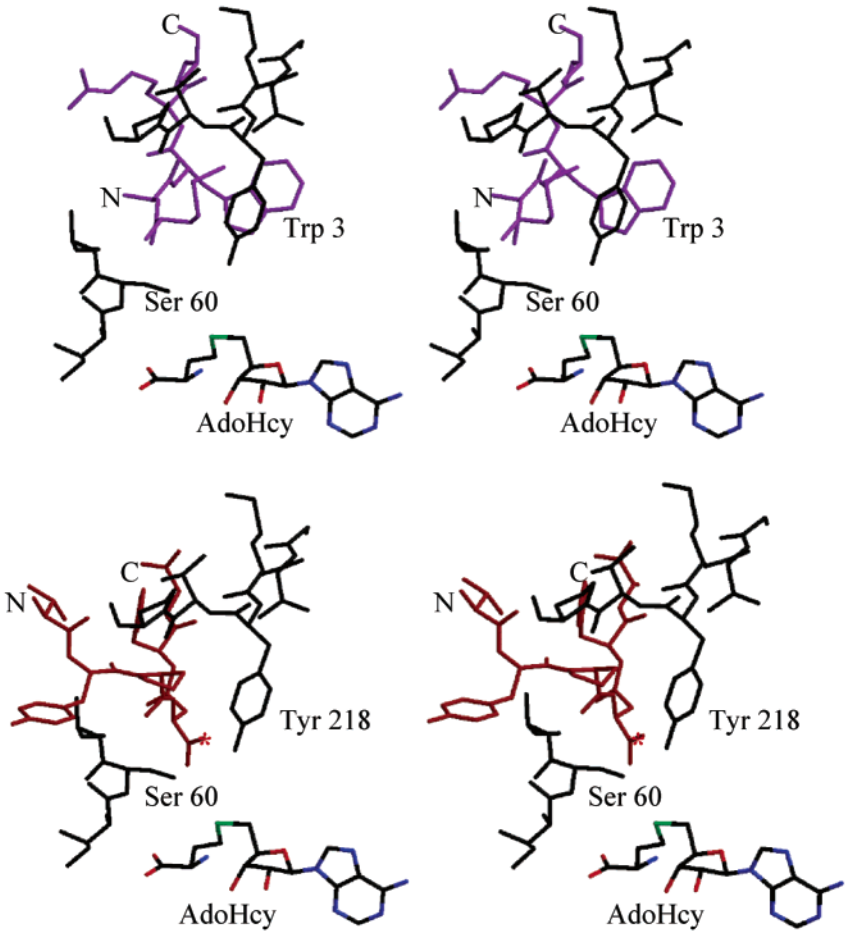

FIGURE 3: The lattice interaction between dPIMT and a crystallographic symmetry-related molecule (top panel) is expected to be similar to that of dPIMT with a peptide substrate modeled into its active site (bottom panel). In both cases, the peptide assumes a conformation so that it comes close to the AdoHcy end product and to Ser-60. In the former case, the Nϵ1 nitrogen of Trp-3 from a neighboring monomer is 5.9 Å from the sulfur atom of the AdoHcy cofactor. In the case of the peptide substrate model, the isoaspartyl carboxylate side chain is positioned so that it can hydrogen bond with the side chain of Ser-60 and the main chain nitrogen of Val-219, bringing the substrate to within 4 Å of the sulfur atom of AdoMet.

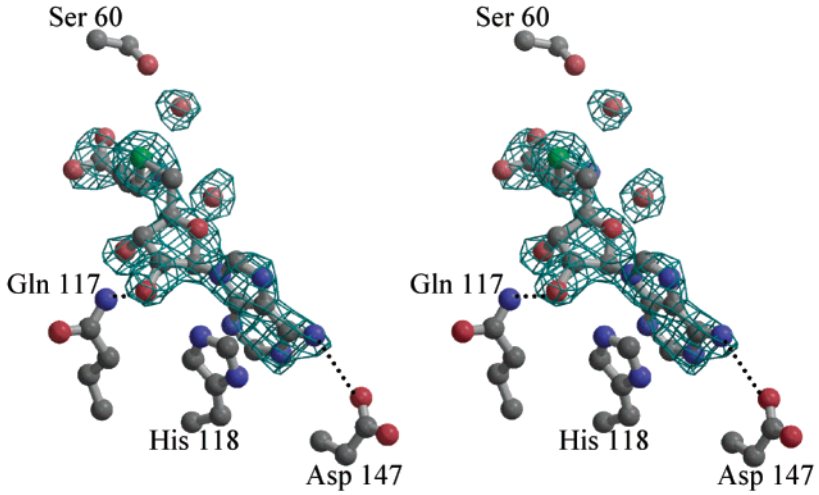

FIGURE 4: Electron density of AdoHcy and surrounding residues. A model of AdoHcy is superimposed upon a $F_o - F_c$ simulated annealing omit map contoured at 3σ. The catalytically important Ser-60 is shown above and forms a hydrogen bond with a water molecule that in turn is hydrogen-bonded to the sulfur atom of AdoHcy. The end product forms a hydrogen bond with Gln-117 in dPIMT, whereas an equivalent hydrogen bond between AdoHcy and Gln-221 is present in human PIMT.

for the S60A enzyme are not shown, because this substitution reduces methyltransferase activity to undetectable levels with either substrate. By contrast, substitution of polar residues for Ser-60 reduces PIMT activity to various extents. The most conservative substitution involving Thr causes a slight reduction in activity with the peptide substrate and a larger reduction with ovalbumin as substrate. Substitution of Gln for Ser-60 has a more profound effect on catalytic activity

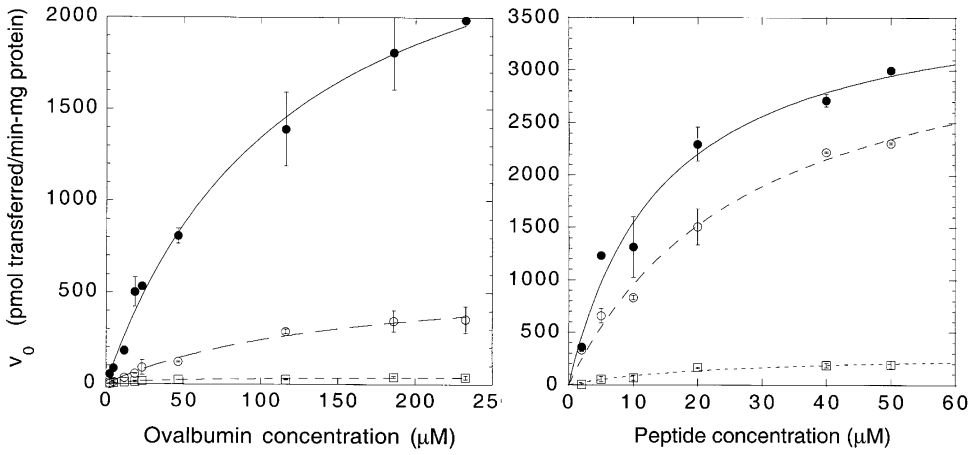

FIGURE 5: Kinetics of ovalbumin and VYP(isoD)HA methylation by wild-type and mutant dPIMTs. Rates of ovalbumin (left panel) and VYP(isoD)HA (right panel) methylation by recombinant wild-type (closed circles), S60T (open circles), and S60Q (open squares) dPIMT were measured as described in Experimental Procedures. Points reflect the average of duplicate determinations with standard errors. In cases where standard errors are not visible, the error was sufficiently small that it is obscured by the symbol. Velocity data are expressed as picomoles of methyl groups transferred per minute per milligram of protein.

Table 2: Kinetic Constants of Wild-Type and Mutant PIMTs with Isoaspartyl Substrates[a]

PIMT	K_m (μM)	V_{max} (pmol min^{-1} mg^{-1})	k_{cat}/K_m (M^{-1} s^{-1})
	Ovalbumin Substrate		
WT	121 ± 17	2980 ± 194	10.2
S60T	159 ± 35	624 ± 69	1.64
S60Q	42.3 ± 10.3	43.6 ± 3.6	0.42
S60A	—[b]	—[b]	
	KASA(isoD)LAKY Substrate		
WT	14.5 ± 3.2	3800 ± 306	109
S60T	28.6 ± 5.3	3690 ± 322	53.7
S60Q	23.0 ± 11.9	292 ± 66	5.29
S60A	—[b]	—[b]	

[a] Enzyme assays were performed as described in Experimental Procedures. Values were determined by fitting the data points to the Michaelis−Menten equation using a nonlinear regression. [b] No activity was detected using the S60A mutant of dPIMT.

of PIMT. The velocity of the reaction is severely reduced, although the enzyme can be saturated with substrate, indicating that ovalbumin and peptide substrates can still bind to the mutant enzymes.

Kinetic parameters for the wild-type and mutant enzymes, summarized in Table 2, were determined by fitting the data points in Figure 5 to the Michaelis−Menten equation. The kinetic parameters of wild-type dPIMT with both substrates fall within the range of values calculated for PIMTs from other eukaryotic sources (*17*). As shown in Table 2, isoaspartyl peptides are better substrates than ovalbumin for both the wild-type and mutant enzymes, possibly because their smaller size and greater conformational flexibility promote binding to PIMT. The relatively conservative substitution of Ser-60 with Thr reduces either the turnover of PIMT or its affinity for substrates, depending on the substrate employed. The more severe substitution of Ser-60 with Gln reduces the specificity constant (k_{cat}/K_m) of the reaction to 4−5% of the wild-type value, primarily by lowering the turnover of the enzyme. The decreased activities of the mutant enzymes are not the effect of improper folding, as indicated by the similarities in the CD spectra and thermal denaturation curves for the mutant and wild-type PIMTs (data not shown).

DISCUSSION

The structural similarity of dPIMT to PIMTs previously described from humans (*20*, *21*) and extreme thermophiles (*22*, *23*) indicates strong evolutionary conservation and is consistent with a fundamental role for PIMT in cellular metabolism. Like other PIMTs characterized to date, dPIMT possesses a central β sheet with a 3↑2↑1↑4↑5↑6↓7↑ topology. This topology, first discovered in the *T. maritima* PIMT (*22*), is now accepted as characteristic of MTases with a specificity for isoaspartyl substrates (*39*). The topological arrangement of the central β sheet in PIMTs differs from that in most other AdoMet-dependent MTases with different substrate specificities in the positions of strands 6 and 7. There are several unique features of dPIMT. The fly enzyme possesses a surface loop, $V_{105}DADT_{109}$, of unknown functional significance that is found in no other PIMT. The other striking difference in the dPIMT structure is the orientation of the C-terminus, which is displaced approximately 90° relative to the positions of the C-termini of the *P. furiosa*, *T. maritima*, and human enzymes. As a consequence, the C-terminal conformation is much more open than in other PIMT structures, and significantly more of the bound AdoHcy is exposed to solvent. This result may provide insight into structural transitions involved in the binding of peptide and protein substrates to PIMTs during a catalytic cycle.

Substrate Binding and Catalysis. Isoaspartyl peptide substrates are known to bind to PIMT near the cofactor binding site on the basis of both modeling experiments (*20*, *22*) and a cocrystal structure (*23*) of the peptide VYP-(isoAsp)HA, adenosine, and *P. furiosus* PIMT. In the *P. furiosus* structure, the isoAsp carboxylate side chain is oriented by two hydrogen bonds. The first bond occurs between its O1 atom and the hydroxyl side chain of the Ser residue homologous to Ser 60 in dPIMT, and the second occurs between its O2 atom and the backbone nitrogen of Val-219. Docking experiments indicate that this brings the O1 atom of isoAsp to ≈3.9 Å from the sulfur atom of a bound AdoHcy or AdoMet ligand. This same peptide geometry can to a large degree be maintained in dPIMT when the bound peptide from the *P. furiosus* complex is super-

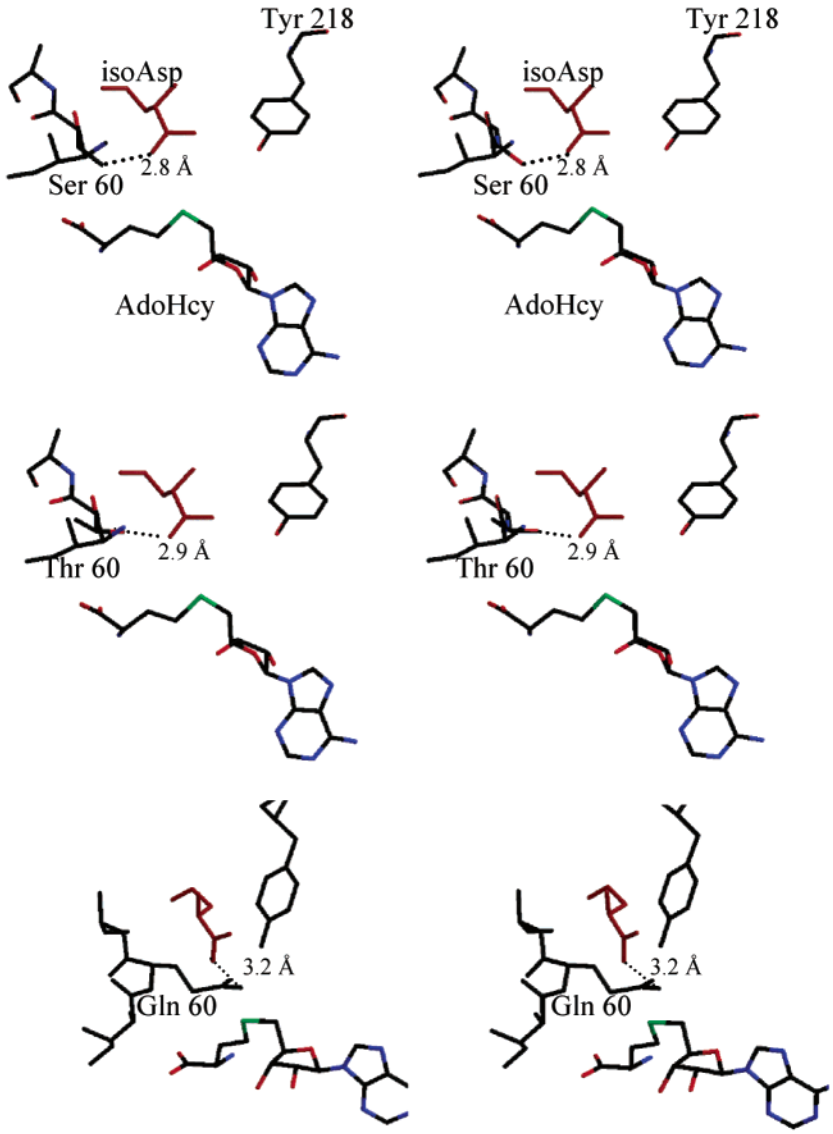

FIGURE 6: The crystal structure of wild-type PIMT (top) and the homology models of S60T (middle) and S60Q (bottom) are presented with the peptide substrate modeled (*33*) as in the bottom panel of Figure 2. The two mutant dPIMT models were constructed with the computer software O (*33*). The S60T and S60Q mutations were initially introduced into dPIMT on the basis of the preferred rotamers. The χ1 (S60T) or both the χ1 and χ2 angles (S60Q) were manually adjusted to minimize poor steric contacts. The hydroxyl group of Thr-60 is rotated to minimize steric clashes, thereby weakening its hydrogen bond with the peptide substrate. The side chain of Gln-60 can also form a hydrogen bond but with a different orientation than what is observed in wild-type PIMT.

imposed upon the dPIMT structure. In the model shown in Figure 3, the last three residues of VYP(isoAsp)HA, which are most important for substrate specificity, fit nicely into dPIMT with no bad contacts. The first three residues clash with the last two residues of dPIMT, however, suggesting that the current conformation of the C-terminal end of dPIMT might restrict substrate binding (see below). Despite these steric clashes, the peptide substrate modeled into dPIMT orients the isoAsp side chain so that the hydrogen-bonding scheme found in *P. furiosus* PIMT is maintained. Ser-60 orients the O1 atom of the isoAsp so that it is closest to the expected position of the methyl group from AdoMet. The environment within the PIMT active site lacks acidic or basic residues immediately around the substrate-binding cleft. This creates an aprotic environment that is favorable for an S_N2 reaction (*40*). Thus, the catalytic power of PIMT derives from its ability both to bring the two substrates together with the right orientation and to increase the mutual attraction of the substrates by creating a favorable environment for the reaction.

Site-directed mutagenesis supports the importance of Ser-60 in catalysis. Substitutions of Thr, Gln, and Ala at this position successively reduce the catalytic efficiency of dPIMT. Modeling of the mutant side chains into the dPIMT structure suggests a possible explanation for these effects (Figure 6). The most severe substitution, S60A, totally removes the possibility of a hydrogen bond between the side chain and the isoAsp substrate and would thereby prevent the substrate from obtaining the orientation necessary for an S_N2 reaction. The lack of a hydrogen bond to an Ala side chain might also reduce the charge distribution on the O1 oxygen of the isoAsp carboxylate group, decreasing its nucleophilicity. In contrast, the introduction of Thr at position 60 has a smaller effect on the kinetic properties of the mutant enzyme relative to wild type. In the S60T mutant, the hydroxyl group still hydrogen bonds with the substrate, even

though the additional methyl group in the side chain has caused it to rotate away from the substrate. This results in a mutant PIMT with restricted freedom of rotation around the χ1 angle of Thr-60. The strength of a hydrogen bond between Thr-60 and a substrate might be expected to depend on the size and flexibility of the substrate. The bond between Thr-60 and a small, flexible peptide could well be similar to that of the wild-type Ser-60 bond, while weaker bonds would be expected between Thr-60 and isoAsp residues in less flexible substrates because the substrate cannot adjust to form an ideal hydrogen bond with Thr-60. In fact, this may explain the reduced catalytic efficiency, reflected in k_{cat}/K_m, of the S60T mutant with ovalbumin rather than the peptide substrate (Table 2).

The substitution of a Gln has a more severe effect on the catalytic mechanism than a Thr substitution but still results in an active enzyme. A model of the S60Q mutant with bound peptide substrate (Figure 6) suggests that this residue can still adopt a conformation that allows a hydrogen bond to be formed with the isoAsp substrate, while avoiding significant steric clashes with the protein. Although the expected hydrogen bond would be weaker than that observed in the wild-type enzyme, the bond should not be significantly weaker than its counterpart in the S60T mutation. The size of the Gln side chain may significantly affect the geometry of the bound substrates, however, such that they are no longer optimally oriented for an S_N2 reaction. In addition, the Gln side chain is closer to the reaction site in this modeled conformation, and its presence could alter the local environment.

Alternative C-Terminal Conformations. Compared to other PIMTs, the C-terminus of dPIMT assumes a much more open conformation that allows more access to the cofactor binding site. The largely hydrophobic coil $M_{217}YVPL_{221}$ is displaced 90° from its counterparts in the other PIMT structures. This sequence, which is highly conserved, forms one ridge of the substrate binding cleft in PIMTs and has numerous contacts with a bound isoaspartyl peptide and cofactors in the *P. furiosus* cocrystal (*23*). The open conformation might result from either the invasion of the N-terminal region of a neighboring monomer or because the natural flexibility of the C-terminal region is stabilized by the observed crystal contacts. In either case, it seems likely that the dPIMT could adopt the more closed conformation observed in other PIMT structures. Our refined *B*-factor model suggests that the C-terminus of dPIMT is flexible enough to adjust to a number of peptide conformations, since the binding modes of an isoaspartyl peptide substrate modeled into the dPIMT structure and the crystallographically related N-terminal sequence are very similar (Figure 3). Consistent with this flexibility, the C-terminus of dPIMT has a higher temperature factor than much of the molecule, and the last five amino acids are not observed in the electron density, presumably because of this disorder. The relatively short C-terminus of dPIMT may contribute to this flexibility. In dPIMT, only three amino acids follow the conserved substrate binding region. By contrast, human PIMT has six more amino acids at the C-terminus than the fly enzyme, and the engineered *P. furiosus* enzyme (*23*) has an additional nine amino acids at the C-terminus, including six His residues used as a purification tag. In both the human and *P. furiosus* enzymes, the C-terminus folds back over the cofactor binding site, limiting solvent access to 0.5% and 1.4% of the respective AdoHcy surface area in the two structures. By contrast, 9% of the AdoHcy surface is accessible to solvent in the fly PIMT structure.

Because the C-terminal residues are involved in both AdoHcy and isoaspartyl peptide binding, it has been proposed that the C-terminus undergoes conformational changes that allow product release and substrate binding (*20*). In solution, PIMT may exist in equilibrium between a closed, human-like conformation and an open, flylike conformation. The open conformation would facilitate the exchange of the AdoHcy end product and the AdoMet substrate, whereas the closed conformation would facilitate the binding of isoAsp-containing substrates while dehydrating the active site. Both the structural data and kinetic experiments suggest that PIMT uses a sequential mechanism that involves multiple conformational states of the enzyme, although there is disagreement on the order of substrate binding and product release. Kinetic experiments first supported a rapid equilibrium random sequential bi-bi mechanism (*41*). The structural data, however, appear more consistent with an ordered mechanism. Based on the geometry of the substrate-binding sites for AdoMet and peptide substrates, earlier structural studies (*20*, *22*) have suggested that PIMT uses an ordered sequential mechanism in which AdoMet binding precedes peptide binding and in which methylated peptide release precedes AdoHcy release. The structure of dPIMT provides a view of an open conformation that is potentially important in the catalytic mechanism. Further work is required to determine which conformation(s) dPIMT adopts in solution.

ACKNOWLEDGMENT

We are grateful to Dr. Martha Teeter for assistance in the initial crystallization experiments.

REFERENCES

1. Kagan, R. M., McFadden, H. J., McFadden, P. N., O'Connor, C., and Clarke, S. (1997) *Comp. Biochem. Physiol. 117B*, 379−385.
2. Ichikawa, J. D., and Clarke, S. (1998) *Arch. Biochem. Biophys. 358*, 222−231.
3. Geiger, T., and Clarke, S. (1987) *J. Biol. Chem. 262*, 785−794.
4. Ota, I. M., and Clarke, S. (1989) *Biochemistry 28*, 4020−4027.
5. Potter, S. M., Henzel, W. J., and Aswad, D. W. (1993) *Protein Sci. 2*, 1648−1663.
6. Johnson, B. A., Langmack, E. L., and Aswad, D. W. (1987) *J. Biol. Chem. 262*, 12283−12287.
7. Hsu, Y.-R., Chang, W.-C., Mendiaz, E. A., Hara, S., Chow, D. T., Mann, M. B., Langley, K. E., and Lu, H. S. (1998) *Biochemistry 37*, 2251−2262.
8. Johnson, B. A., Murray, E. D., Jr., Clarke, S., Glass, D. B., and Aswad, D. W. (1987) *J. Biol. Chem. 262*, 5622−5629.
9. McFadden, P. N., and Clarke, S. (1987) *Proc. Natl. Acad. Sci. U.S.A. 84*, 2595−2599.
10. Brennan, T. V., Anderson, J. W., Jia, Z., Waygood, E. B., and Clarke, S. (1994) *J. Biol. Chem. 269*, 24586−24595.
11. O'Connor, C. M., and Clarke, S. (1985) *Anal. Biochem. 148*, 79−85.
12. Barber, J. R., and Clarke, S. (1983) *J. Biol. Chem. 258*, 1189−1196.
13. O'Connor, C. M., and Clarke, S. (1984) *J. Biol. Chem. 259*, 2570−2578.
14. Szymanska, G., Leszyk, J. D., and O'Connor, C. M. (1998) *J. Biol. Chem. 273*, 28516−28523.
15. Kim, E., Lowenson, J. D., MacLaren, D. C., Clarke, S., and Young, S. G. (1997) *Proc. Natl. Acad. Sci. U.S.A. 94*, 6132−6137.
16. Yamamoto, A., Takagi, H., Kitamura, D., Tatsuoka, H., Nakano, H., Kawano, H., Kuroyanagi, H., Yahagi, Y., Kobayashi, S., Koizumi, K., Sakai, T., Saito, K., Chiba, T., Kawamura, K.,

Suzuki, K., Watanabe, T., Mori, H., and Shirasawa, T. (1998) *J. Neurosci. 18*, 2063−2074.
17. Kagan, R. M., Niewmierzycka, A., and Clarke, S. (1997) *Arch. Biochem. Biophys. 348*, 320−328.
18. Brand, A. H., and Perrimon, N. (1993) *Development 118*, 401−415.
19. Chavous, D. A., Jackson, F. R., and O'Connor, C. M. (2001) *Proc. Natl. Acad. Sci. U.S.A. 98*, 14814−14818.
20. Smith, C. D., Carson, M., Friedman, A. M., Skinner, M. M., Delucas, L., Chantalat, L., Weise, L., Shirasawa, T., and Chattopadhyay, D. (2002) *Protein Sci. 11*, 625−635.
21. Ryttersgaard, C., Griffith, S. C., Sawaya, M. R., MacLaren, D. C., Clarke, S., and Yeates, T. O. (2002) *J. Biol. Chem. 277*, 10642−10646.
22. Skinner, M. M., Puvathingal, J. M., Walter, R. L., and Friedman, A. M. (2000) *Structure 8*, 1189−1201.
23. Griffith, S. C., Sawaya, M. R., Boutz, D. R., Thapar, N., Katz, J. E., Clarke, S., and Yeates, T. O. (2001) *J. Mol. Biol. 313*, 1103−1116.
24. O'Connor, M. B., Galus, A., Hartenstine, M., Magee, M., Jackson, F. R., and O'Connor, C. M. (1997) *Insect Biochem. Mol. Biol. 27*, 49−54.
25. Henzel, W. J., Stults, J. T., Hsu, C.-A., and Aswad, D. W. (1989) *J. Biol. Chem. 264*, 15905−15911.
26. Matthews, B. W. (1968) *J. Mol. Biol. 33*, 491−497.
27. Otwinowski, Z., and Minor, W. (1997) *Methods Enzymol. 276*, 307−326.
28. Collaborative Computational Project Number 4 (1994) *Acta Crystallogr. 50*, 414−423.
29. Navaza, J. (1994) *Acta Crystallogr., Sect. D 50*, 157−163.
30. Brunger, A. T., Adams, P. D., Clore, G. M., DeLano, W. L., Gros, P., Grosse-Kunstleve, R. W., Jiang, J. S., Kuszewski, J., Nilges, M., Pannu, N. S., Read, R. J., Rice, L. M., Simonson, T., and Warren, G. L. (1998) *Acta Crystallogr., Sect. D 54*, 905−921.
31. Hodel, A., Kim, S.-H., and Brunger, A. T. (1992) *Acta Crystallogr., Sect. A 48*, 851−858.
32. Read, R. J. (1986) *Acta Crystallogr., Sect. A 42*, 140−149.
33. Jones, T. A., Zou, J.-Y., Cowan, S. W., and Kjeldgaard, M. (1991) *Acta Crystallogr., Sect. A 47*, 110−119.
34. Korostelev, A., Bertram, R., and Chapman, M. S. (2002) *Acta Crystallogr., Sect. D 58*, 946−950.
35. Kleywegt, G. J. (1996) *Acta Crystallogr., Sect. D 52*, 842−857.
36. Collaborative Computational Project Number 4 (1994) *Acta Crystallogr., Sect. D 50*, 760−763.
37. O'Connor, C. M. (1987) *J. Biol. Chem. 262*, 10398−10403.
38. Deng, W. P., and Nickoloff, J. A. (1992) *Anal. Biochem. 200*, 81−88.
39. Martin, J. L., and McMillan, F. M. (2002) *Curr. Opin. Struct. Biol. 12*, 783−793.
40. Parker, A. J. (1969) *Chem. Rev. 69*, 1−32.
41. Johnson, B. A., and Aswad, D. W. (1993) *Neurochem. Res. 18*, 87−94.
42. Laskowski, R. A., MacArthur, M. W., Moss, D. S., and Thornton, J. M. (1993) *J. Appl. Crystallogr. 24*, 946−950.
43. Esnouf, R. M. (1997) *J. Mol. Graphics Modell. 15*, 132−134.
44. Merritt, E. A., and Bacon, D. J. (1997) *Methods Enzymol. 277*, 505−524.

BI034891+